# CHAPTER IV
# RESULTS AND DISCUSSION

In a plasma environment, the highly energetic electrons generated by gliding arc discharge collide with the gaseous molecules of hydrocarbons, $CO_2$, $O_2$ and $H_2O$ creating a variety of chemically active radicals. All the possibilities of chemical pathways occurring under the studied conditions are briefly described below to provide a better comprehensive understanding of the combined steam reforming and partial oxidation of $CO_2$-containing natural gas in gliding arc discharge plasma. The radicals of oxygen active species are produced during the collisions between electrons and $CO_2$, as shown in Eqs. 4.1 and 4.2. Moreover, the produced CO can be further dissociated by the collision with electrons to form coke and oxygen active species (Eq. 4.3). In the case of added oxygen, a large amount of oxygen active species can be produced from the collisions between electrons and oxygen molecules, as described by Eqs. 4.4-4.6. The collisions between electrons and all hydrocarbons presented in the feed to produce hydrogen and various hydrocarbon species for subsequent reactions are described by Eqs. 4.7-4.19.

Electron-carbon dioxide collisions:

$$e^- + CO_2 \rightarrow CO + O^- \quad (4.1)$$

$$e^- + CO_2 \rightarrow CO + O + e^- \quad (4.2)$$

$$e^- + CO \rightarrow C + O + e^- \quad (4.3)$$

Electron-oxygen collisions:

$$e^- + O_2 \rightarrow 2O + e^- \rightarrow O^- + O \quad (4.4)$$

$$e^- + O_2 \rightarrow O_2^- \quad (4.5)$$

$$e^- + O_2 \rightarrow 2O + e^- \quad (4.6)$$

Electron-methane collisions:

$$e^- + CH_4 \rightarrow CH_3 + H + e^- \quad (4.7)$$

$$e^- + CH_3 \rightarrow CH_2 + H + e^- \quad (4.8)$$

$$e^- + CH_2 \rightarrow CH + H + e^- \quad (4.9)$$

$$e^- + CH \rightarrow C + H + e^- \quad (4.10)$$

$$H + H \rightarrow H_2 \quad (4.11)$$

Electron-ethane collisions:

$$e^- + C_2H_6 \rightarrow C_2H_5 + H + e^- \quad (4.12)$$

$$e^- + C_2H_5 \rightarrow C_2H_4 + H + e^- \quad (4.13)$$

$$e^- + C_2H_4 \rightarrow C_2H_3 + H + e^- \quad (4.14)$$

$$e^- + C_2H_3 \rightarrow C_2H_2 + H + e^- \quad (4.15)$$

$$e^- + C_2H_6 \rightarrow CH_3 + CH_3 + e^- \quad (4.16)$$

Electron-propane collisions:

$$e^- + C_3H_8 \rightarrow C_3H_7 + H + e^- \quad (4.17)$$

$$e^- + C_3H_7 \rightarrow C_3H_6 + H + e^- \quad (4.18)$$

$$e^- + C_3H_8 \rightarrow C_2H_5 + CH_3 + e^- \quad (4.19)$$

The oxygen active species derived from $CO_2$ and $O_2$ can further extract hydrogen atoms from the molecules of hydrocarbon gases via the oxidative dehydrogenation reactions (Eqs. 4.20-4.33), consequently producing several chemically active radicals and water.

Oxidative dehydrogenation reactions:

$$CH_4 + O \rightarrow CH_3 + OH \quad (4.20)$$

$$C_2H_6 + O \rightarrow C_2H_5 + OH \quad (4.21)$$

$$C_2H_5 + O \rightarrow C_2H_4 + OH \quad (4.22)$$

$$C_2H_4 + O \rightarrow C_2H_3 + OH \quad (4.23)$$

$$C_2H_3 + O \rightarrow C_2H_2 + OH \quad (4.24)$$

$$C_3H_8 + O \rightarrow C_3H_7 + OH \quad (4.25)$$

$$C_3H_7 + O \rightarrow C_3H_6 + OH \quad (4.26)$$

$$CH_4 + OH \rightarrow CH_3 + H_2O \quad (4.27)$$

$$C_2H_6 + OH \rightarrow C_2H_5 + H_2O \quad (4.28)$$

$$C_2H_5 + OH \rightarrow C_2H_4 + H_2O \quad (4.29)$$

$$C_2H_4 + OH \rightarrow C_2H_3 + H_2O \quad (4.30)$$

$$C_2H_3 + OH \rightarrow C_2H_2 + H_2O \quad (4.31)$$

$$C_3H_8 + OH \rightarrow C_3H_7 + H_2O \quad (4.32)$$

$$C_3H_7 + OH \rightarrow C_3H_6 + H_2O \quad (4.33)$$

The $C_2H_5$, $C_2H_3$, and $C_3H_7$ radicals can further react to form ethylene, acetylene, and propene either by electron collisions (Eqs. 4.13-4.15, and 4.18) or by oxidative dehydrogenation reactions (Eqs. 4.22-4.24, 4.26-4.29, 4.31, and 4.33). The extracted hydrogen atoms immediately form hydrogen gas according to Eq. 4.11. However, no propene was detected in the outlet gas stream. It is therefore believed that the propene species is unstable and may possibly undergo further reactions (Eqs. 4.34 and 4.35).

Propene hydrogenation and cracking reactions:

$$C_3H_6 + H_2 \rightarrow C_3H_8 \quad (4.34)$$

$$C_3H_6 \rightarrow C_2H_2 + CH_4 \quad (4.35)$$

In addition, the radicals of hydrocarbons and hydrogen derived from the earlier reactions react further to combine with one another via coupling reactions to form ethane, ethylene, acetylene, propane, and butane, as shown in Eqs. 4.36-4.51. In addition, ethane can be further dehydrogenated to form ethylene, while ethylene can also be dehydrogenated to form acetylene by either electron collisions or oxidative dehydrogenation reactions (Eqs. 4.12, 4.13, 4.21, 4.22, 4.28, and 4.29 for ethylene formation; and, Eqs. 4.14, 4.15, 4.23, 4.24, 4.30, and 4.31 for acetylene formation).

Coupling reactions of active species:

*Ethane formation;*

$$CH_3 + CH_3 \rightarrow C_2H_6 \quad (4.36)$$

$$C_2H_5 + H \rightarrow C_2H_6 \quad (4.37)$$

$$C_2H_5 + C_2H_5 \rightarrow C_2H_6 + C_2H_4 \quad (4.38)$$

$$C_3H_7 + CH_3 \rightarrow C_2H_6 + C_2H_4 \quad (4.39)$$

*Ethylene formation;* $CH_2 + CH_2 \rightarrow C_2H_4$ (4.40)

$CH_3 + CH_3 \rightarrow C_2H_4 + H_2$ (4.41)

$C_2H_5 + H \rightarrow C_2H_4 + H_2$ (4.42)

$C_3H_7 + H \rightarrow C_2H_4 + CH_4$ (4.43)

*Acetylene formation;* $CH + CH \rightarrow C_2H_2$ (4.44)

$CH_2 + CH_2 \rightarrow C_2H_2 + H_2$ (4.45)

$CH_3 + CH \rightarrow C_2H_2 + H_2$ (4.46)

$C_2H_5 + H \rightarrow C_2H_2 + H_2 + H_2$ (4.47)

$C_3H_7 + H \rightarrow C_2H_2 + CH_4 + H_2$ (4.48)

*Propane formation;* $C_2H_5 + CH_3 \rightarrow C_3H_8$ (4.49)

*Butane formation;* $C_2H_5 + C_2H_5 \rightarrow C_4H_{10}$ (4.50)

$C_3H_7 + CH_3 \rightarrow C_4H_{10}$ (4.51)

Moreover, a significant amount of CO and a very small amount of water were produced under the studied conditions, particularly in feed with high oxygen content. CO may be mainly formed via the $CO_2$ dissociation (Eqs. 4.1 and 4.2). Eqs. 4.52-4.56 show the partial oxidative pathways of methyl radical to form CO and $H_2$ as the end products. The formation of water is believed to occur via the oxidative hydrocarbon reactions (Eqs. 4.27-4.33). In addition, water can be formed by the reactions between hydrogen or hydrogen active radical and oxygen active radical, as shown in Eqs. 4.57-4.59.

Carbon monoxide formation:

$CH_3 + O \rightarrow HCHO$ (4.52)

$HCHO + O \rightarrow OH + CHO$ (4.53)

$CHO + O \rightarrow OH + CO$ (4.54)

$CHO + OH \rightarrow CO + H_2O$ (4.55)

$CHO + H \rightarrow H_2 + CO$ (4.56)

Water formation:

$$2H + O \rightarrow H_2O \quad (4.57)$$

$$H_2 + O \rightarrow H_2O \quad (4.58)$$

$$H_2 + ½\,O \rightarrow H_2O \quad (4.59)$$

Additionally, hydrocarbon molecules may crack to form carbon and hydrogen via cracking reactions (Eqs. 4.60-4.62).

$$CH_4 \rightarrow C + 2H_2 \quad (4.60)$$

$$C_2H_6 \rightarrow 2C + 3H_2 \quad (4.61)$$

$$C_3H_8 \rightarrow 3C + 4H_2 \quad (4.62)$$

Moreover, water molecule may crack to form hydrogen via dissociation reactions (Eqs. 4.63 and 4.64).

$$e^- + H_2O \rightarrow O^- + H_2 \quad (4.63)$$

$$e^- + H_2O \rightarrow OH^- + H \quad (4.64)$$

## 4.1 Effect of Hydrocarbons (HCs)/$O_2$ Feed Molar Ratio

### 4.1.1 Effect on Reactant Conversions and Product Yields

Typically, the hydrocarbons (HCs)/$O_2$ feed molar ratio of the natural gas feed mixture has a considerable impact on the plasma characteristics (i.e. breakdown voltage, electrical conductivity, and physical appearance) and the plasma stability, which in turn, depend on different properties of each gas component. In this research, the experiments were initially performed by varying oxygen content in feed to obtain various HCs/$O_2$ feed molar ratios of 2/1, 3/1, 4/1, 6/1, and 9/1, while the other operating parameters were controlled at a steam content of 10 mol%, a total feed flow rate of 100 $cm^3$/min, an applied voltage of 13.5 kV, an input frequency of 300 Hz, and an electrode gap distance of 6 mm, which were obtained from the previous work (Pornmai, 2008). In this plasma system, a HCs/$O_2$ feed molar ratio lower than 2/1 was not investigated since it is close to the upper explosion limit.

The effect of $HCs/O_2$ feed molar ratio on the reactant conversions and product yields is shown in Figure 4.1(a). The conversions of all reactants, except $CO_2$, as well as the $H_2$, CO, and $C_2$ yields increased with decreasing $HCs/O_2$ feed molar ratio (a lower $HCs/O_2$ feed molar ratio means a higher $O_2$ content). Basically, in the plasma system, the oxygen plays an important role in providing oxygen active species from its dissociation reactions via the collision by electrons (Eqs. 4.4-4.6). These active species can activate all reactants to form various products by increasing the rates of oxidative dehydrogenation reactions and coupling reactions (Eqs. 4.20-4.33 and 4.36-4.51), leading to the increases in the conversions of $CH_4$, $C_2H_6$, and $C_3H_8$, as well as the $H_2$ and $C_2$ yields. These results well relate to the decreases in $CH_4$, $C_2H_6$, and $C_3H_8$ concentrations, as well as the increases in $H_2$ and CO concentrations in the outlet gas, when decreasing $HCs/O_2$ feed molar ratio (Figure 4.1(b)). This is because a large oxygen content can alter the plasma characteristic and increase the plasma stability, which could be directly observed from the discharge appearance and its behaviors (e.g. a higher number of arcs produced with smooth arc patterns along the knife-shaped electrode pairs). In comparison between the cases without and with $O_2$ addition in feed, the $O_2$ addition in feed with the $HC/O_2$ feed molar ratio of 2/1 potentially contributed the positive effect to the enhancement of the reactant conversions and the $H_2$, CO, and $C_2$ yields. Incontrast, the $CO_2$ conversion decreased with decreasing $HCs/O_2$ feed molar ratio. The negative $CO_2$ conversion can be explained in that the formation rate of $CO_2$ by the hydrocarbon oxidation is higher than the $CO_2$ consumption rate by the reforming reactions (Rueangjitt *et al.*, 2008).

4.1.2 Effect on Product Selectivities and Product Molar Ratios

Figure 4.2(a) shows the effect of $HCs/O_2$ feed molar ratio on product selectivities. The selectivities for $C_2H_4$, $C_4H_{10}$, and $H_2$ tended to decrease with decreasing $HCs/O_2$ feed molar ratio, whereas the selectivity for CO increased. At a low $HCs/O_2$ feed molar ratio, more availability of oxygen active species is responsible for more opportunity for oxidative dehydrogenation reactions (Eqs. 4.20-4.33) and CO formation (Eqs. 4.52-4.56). Conversely, the opportunity for coupling reactions to form $C_2H_4$ and $C_4H_{10}$, as well as $H_2$, is less favorable at lower $HCs/O_2$ feed molar ratios (Esq. 4.40-4.43 and 4.50-4.51). This explanation is also confirmed by the results of product ratios. Figure 4.2(b) shows the effect of $HCs/O_2$ feed molar ratio on the product molar ratios. The molar ratios of $H_2/CO$, $H_2/C_2H_2$, and $C_2H_4/C_2H_2$ decreased with decreasing $HCs/O_2$ feed molar ratio, while the $H_2/C_2H_4$ molar ratio showed the opposite trend. These results well correspond to the decreased $C_2H_4$, $C_4H_{10}$, and $H_2$ selectivities and the increased CO selectivity. These results confirm that the oxidative dehydrogenation reactions of hydrocarbons and electron-carbon dioxide collision reactions have higher possibilities to occur, as compared to the coupling reactions of active species.

4.1.3 Effect on Power Consumptions

Figure 4.3 shows the effect of $HCs/O_2$ feed molar ratio on power consumptions and coke formation. The power consumptions both per reactant molecule converted and per $H_2$ molecule produced decreased with decreasing $HCs/O_2$ feed molar ratio. The decreases in both power consumptions can be explained by the increases in the $CH_4$, $C_2H_6$, and $C_3H_8$ conversions, as well as the $H_2$ yield (Figure 4.1(a)). These results suggest that the power consumption in the plasma steam reforming of simulated natural gas can be significantly reduced by adding oxygen in feed. Moreover, a decreased tendency for coke formation on the electrode surfaces and inner reactor glass wall could be observed at lower $HCs/O_2$ feed molar ratios (with high $O_2$ contents). From the overall results, the optimum $HCs/O_2$ feed molar ratio of 2/1, which reasonably provided both desired product

(systhesis gas) yields and selectivities and relatively low power consumptions, was selected for further experiments.

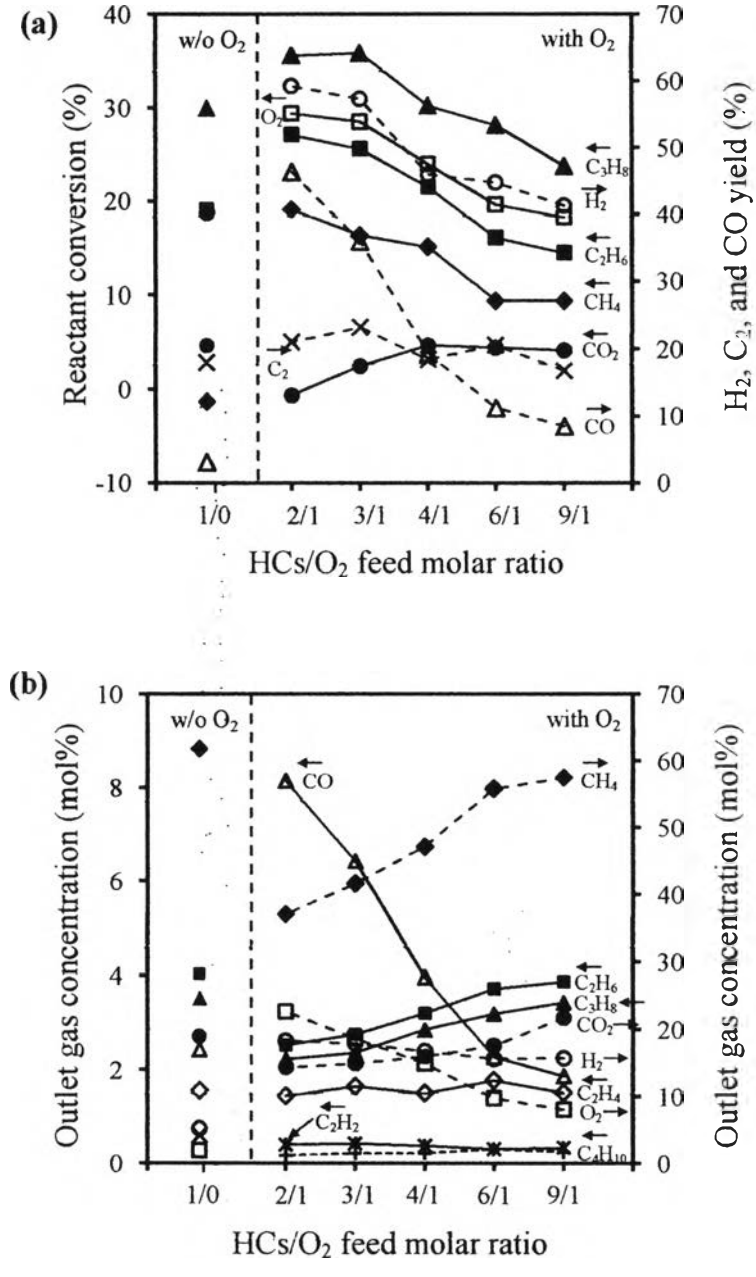


**Figure 4.1** Effect of HCs/$O_2$ feed molar ratio on (a) reactant conversions and product yields and (b) concentrations of outlet gas for the combined steam reforming and partial oxidation of natural gas (steam content, 10 mol%; total feed flow rate, 100 $cm^3$/min; applied voltage, 13.5 kV; input frequency, 300 Hz; and electrode gap distance, 6 mm).

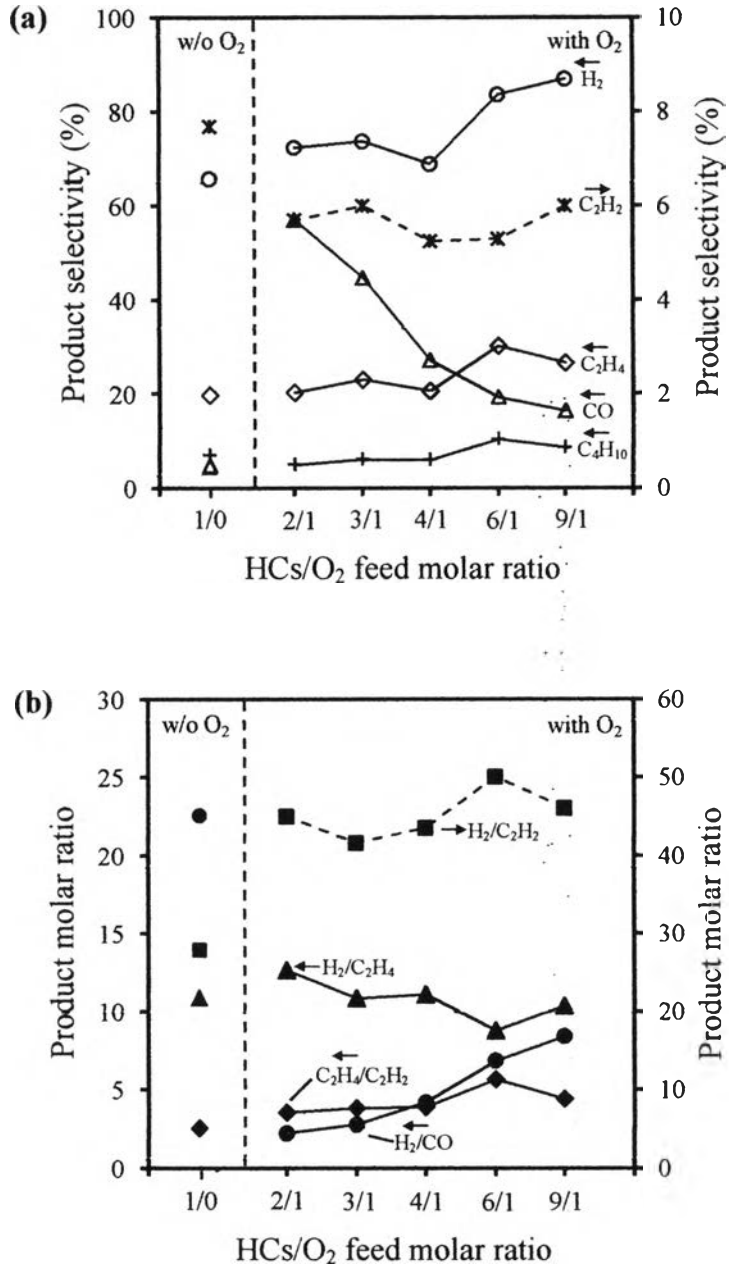


**Figure 4.2** Effect of HCs/$O_2$ feed molar ratio on (a) product selectivities and (b) product molar ratios for the combined steam reforming and partial oxidation of natural gas (steam content, 10 mol%; total feed flow rate, 100 $cm^3$/min; applied voltage, 13.5 kV; input frequency, 300 Hz; and electrode gap distance, 6 mm).

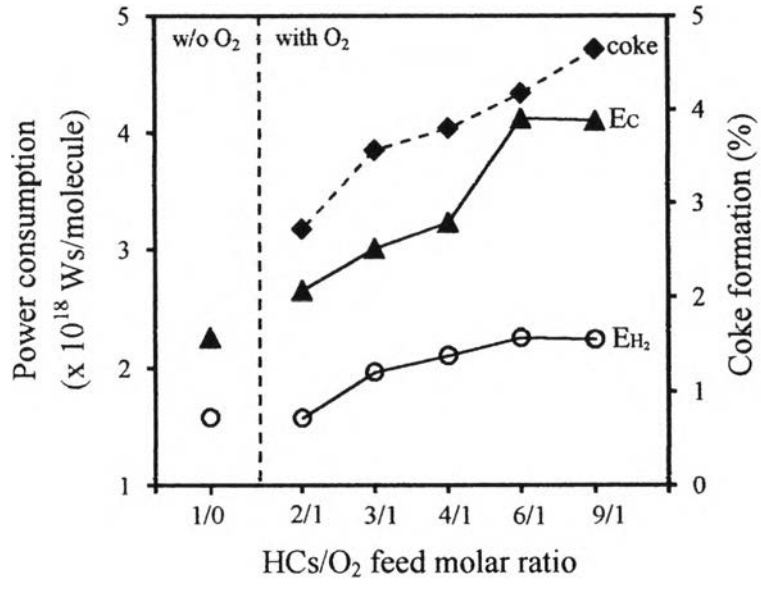


**Figure 4.3** Effect of HCs/$O_2$ feed molar ratio on power consumptions and coke formation for the combined steam reforming and partial oxidation of natural gas (steam content, 10 mol%; total feed flow rate, 100 $cm^3$/min; applied voltage, 13.5 kV; input frequency, 300 Hz; and electrode gap distance, 6 mm) ($E_C$: power per reactant molecule converted; $E_{H2}$: power per $H_2$ molecule produced).

## 4.2 Effect of Applied Voltage

### 4.2.1 Effect on Reactant Conversions and Product Yields

Applied voltage is one of the most important operating parameters in controlling the non-thermal plasma performance. The experiments were next performed to investigate the effect of applied voltage in the range of 13.5 to 20.5 kV, while the other operating parameters were controlled at a steam content of 10 mol%, a $HCs/O_2$ feed molar ratio of 2/1, a total feed flow rate of 100 $cm^3/min$, an input frequency of 300 Hz, and an electrode gap distance of 6 mm. In this plasma system, the highest operating applied voltage of 20.5 kV was limited by the plasma instability and thereby permanent extinction of discharges, whereas the lowest operating applied voltage of 13.5 kV was limited by the insufficient and unstable gliding arc discharges.

The effect of applied voltage on the reactant conversions and product yields is illustrated in Figure 4.4(a). The conversions of all reactants steadily increased with increasing applied voltage. The negative $CO_2$ conversion can be explained by the higher formation rate of $CO_2$ by the hydrocarbon oxidation as compared to the $CO_2$ consumption rate by the reforming reaction, as mentioned above. These results well relate to the decreases in $CH_4$, $C_2H_6$, $C_3H_8$, and $O_2$ concentrations, as well as the increases in $H_2$ and CO concentrations in the outlet gas (Figure 4.4(b)). Basically, an increase in applied voltage for the plasma-chemical reactions contributes directly to stronger electric field strength across the electrodes. As clearly shown in Figure 4.4(c), the generated current increased with increasing applied voltage. More specifically, the electric field strength is simply proportional to the mean electron energy and electron temperature in the plasma. As a result, at a higher applied voltage, the generated plasma possesses not only electrons with a higher average energy and temperature but also a higher electron density. For this reason, the opportunity for the occurrence of elementary chemical reactions with electron impact (mainly ionization, excitation, and dissociation of gas molecules) in non-thermal plasma can be improved by increasing applied voltage. However, the $C_2$ yield remained almost unchanged with increasing applied voltage, suggesting that the $C_2$ yield was independent of an applied voltage.

4.2.2 Effect on Product Selectivities and Product Molar Ratios

Figure 4.5(a) shows the effect of applied voltage on the product selectivities. The $H_2$, $C_2H_4$, and $C_4H_{10}$ selectivities tended to decrease with increasing applied voltage from 13.5 to 20.5 kV, whereas the $C_2H_2$ and CO selectivities tended to increase. These results imply that at a higher applied voltage, the oxidative dehydrogenation reactions (Esq. 4.20-2.33) preferably occur than the coupling reactions of active species (Esq. 4.36-4.51). A possible explanation is that at a higher applied voltage, a higher electron density and a subsequent more number of active species, as mentioned above, lead to the substantial increase in opportunity for oxidative dehydrogenation reactions. Figure 4.5(b) shows the effect of applied voltage on the product molar ratios. The molar ratios of $H_2$/CO, $H_2/C_2H_2$, and $C_2H_4/C_2H_2$ decreased with increasing applied voltage from 13.5 to 20.5 kV, while the $H_2/C_2H_4$ molar ratio showed the opposite trend. These results agree well with the decreased $H_2$, $C_2H_4$, and $C_4H_{10}$ selectivities and the increased $C_2H_2$ and CO selectivities. These results clearly confirm that the oxidative dehydrogenation reactions of hydrocarbons are preferable to occur much more than the coupling reactions of active species.

4.2.3 Effect on Power Consumptions

Figure 4.6 shows the effect of applied voltage on power consumptions and coke formation. The power consumptions both per reactant molecule converted and per $H_2$ molecule produced initially decreased with increasing applied voltage from 13.5 to 14.5 kV and then tended to gradually increase with further increasing applied voltage to 20.5 kV. The initial decrease in both power consumptions can be explained by the increases in the $CH_4$, $C_2H_6$, and $C_3H_8$ conversions and $H_2$ yield (Figure 4.4(a)). By considering the applied voltage range of 14.5 to 20.5 kV, both power consumptions adversely increased, possibly because of the drastic appearance of coke deposition on the electrode surfaces, as clearly seen in Figure 4.6. Hence, the minimum power consumptions were found at the applied voltage of 14.5 kV, which greatly provided both high $H_2$ yield and selectivity; therefore, the applied voltage of 14.5 kV was selected for further experiments.

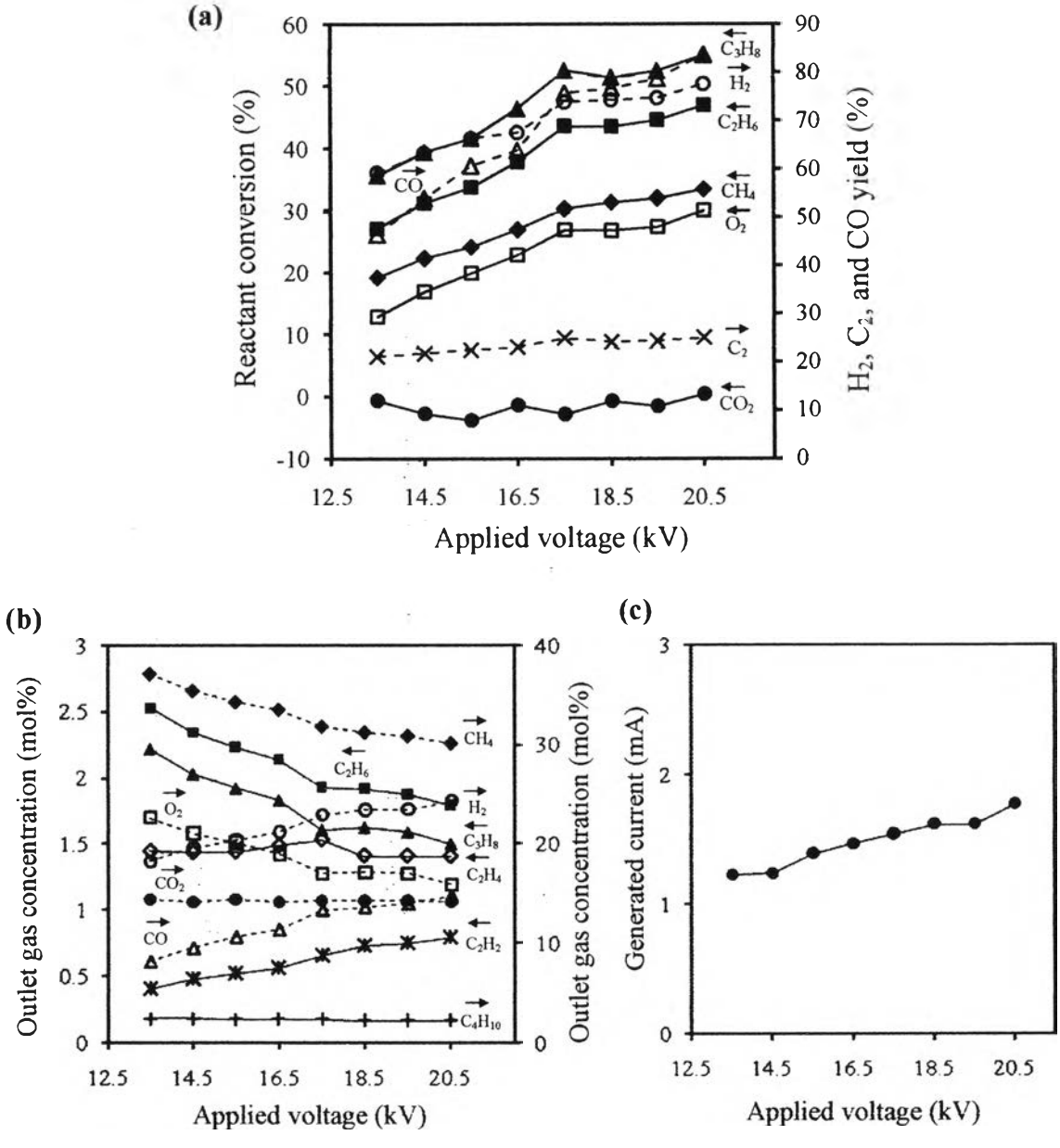


**Figure 4.4** Effect of applied voltage on (a) reactant conversions and product yields, (b) concentrations of outlet gas, and (c) generated current for the combined steam reforming and partial oxidation of natural gas (steam content, 10 mol%; HCs/$O_2$ feed molar ratio of 2/1; total feed flow rate, 100 $cm^3$/min; input frequency, 300 Hz; and electrode gap distance, 6 mm).

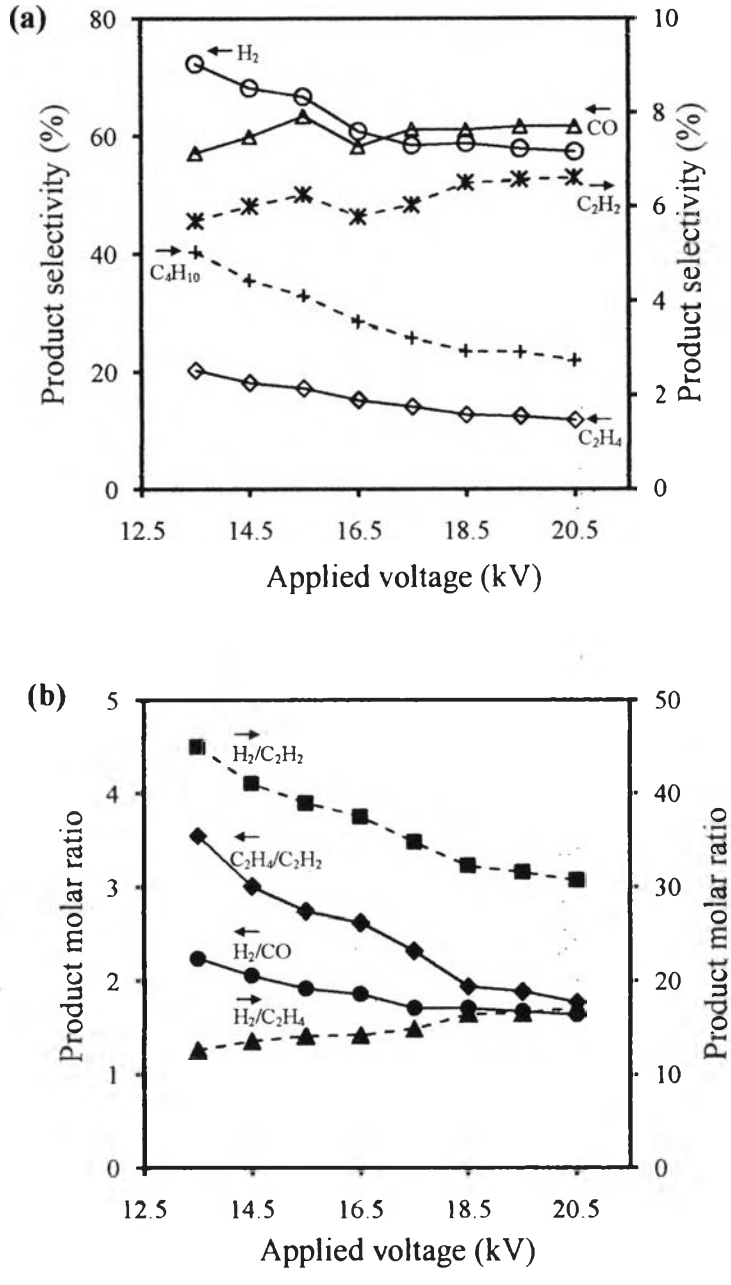


**Figure 4.5** Effect of applied voltage on (a) product selectivities and (b) product molar ratios for the combined steam reforming and partial oxidation of natural gas (steam content, 10 mol%; $HCs/O_2$ feed molar ratio of 2/1; total feed flow rate, 100 $cm^3$/min; input frequency, 300 Hz; and electrode gap distance, 6 mm).

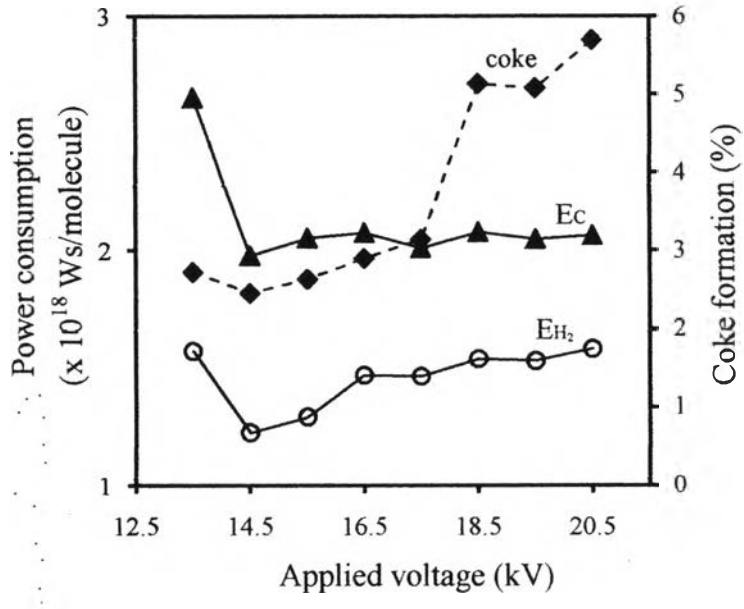


**Figure 4.6** Effect of applied voltage on power consumptions and coke formation for the combined steam reforming and partial oxidation of natural gas (steam content, 10 mol%; $HCs/O_2$ feed molar ratio of 2/1; total feed flow rate, 100 $cm^3$/min; input frequency, 300 Hz; and electrode gap distance, 6 mm) ($E_C$: power per reactant molecule converted; $E_{H2}$: power per $H_2$ molecule produced).

## 4.3 Effect of Input Frequency

### 4.3.1 Effect on Reactant Conversions and Product Yields

For the investigation of the effect of input frequency on the reforming reactions of the simulated natural gas, the frequency parameter was experimentally varied in the range of 290–500 Hz, while the other operating parameters were controlled at a steam content of 10 mol%, a $HCs/O_2$ feed molar ratio of 2/1, a total feed flow rate of 100 $cm^3$/min, an applied voltage of 14.5 kV, and an electrode gap distance of 6 mm. In this plasma system, the highest operating input frequency of 500 Hz was limited by the unstable gliding arc discharges, observed from the discharge appearance and its behavior (e.g. an extremely small number of arcs produced with unsmooth arc patterns along the knife-shaped electrode pairs), whereas the lowest operating input frequency of 290 Hz was limited by the large coke formation on the electrodes.

The effect of input frequency on the reactant conversions and product yields is illustrated in Figure 4.7(a). The conversions of $CH_4$, $C_2H_6$, $C_3H_8$, and $O_2$, as well as the $H_2$, CO, and $C_2$ yields, steadily decreased with increasing input frequency. The negative $CO_2$ conversion can be explained as mentioned before. These results well correspond to the increases in $CH_4$, $C_2H_6$, $C_3H_8$, and $O_2$ concentrations, as well as the decreases in $H_2$ and CO concentrations in the outlet gas (Figure 4.7(b)). Basically, at a constant applied voltage and a fixed electrode gap distance, the electric current needed to initiate and maintain the discharge plasma is reduced with increasing frequency. Consequently, a lower current was generated at a higher frequency, as shown in Figure 4.7(c). Based on the basic concept of the frequency effect as stated, the space charge characteristic of the alternating current discharge is the influential factor of frequency in changing the behaviors of discharge and the reaction performance. Therefore, increasing frequency adversely brings about the reduction in the number of electrons generated for initiating the chemically reactive species via the elementary processes with electron impact and for activating the subsequent chemical reactions, resulting in lower reactant conversions and product yields.

4.3.2 Effect on Product Selectivities and Product Molar Ratios

Figure 4.8(a) shows the effect of input frequency on the product selectivities. The $H_2$, $C_2H_2$, and $C_4H_{10}$ selectivities tended to increase with increasing input frequency from 290 to 500 Hz, whereas the $C_2H_4$ and CO selectivities tended to remain almost unchanged, suggesting that the $C_2H_4$ and CO selectivities were independent of an input frequency. These results imply that at a higher input frequency, the coupling reactions of active species (Esq. 4.36-4.51) more preferably occur as compared to the oxidative dehydrogenation reactions (Esq. 4.20-2.33). They suggest that the promotion of coupling reactions can be attained by increasing the input frequency. Figure 4.8(b) shows the effect of input frequency on the product molar ratios. The molar ratios of $H_2/CO$, $H_2/C_2H_2$, and $C_2H_4/C_2H_2$ tended to increase with increasing input frequency, while the $H_2/C_2H_4$ molar ratio remained almost invariant. These results agree well with the increased $H_2$ and $C_2H_2$ selectivities.

4.3.3 Effect on Power Consumptions

Figure 4.9 shows the effect of input frequency on power consumptions and coke formation. The power consumptions both per reactant molecule converted and per $H_2$ molecule produced initially decreased with increasing input frequency from 290 to 300 Hz and then substantially increased with further increasing input frequency to 500 Hz. The initial decrease in both power consumptions was observed probably due to the decrease in current required to sustain the discharge (Figure 4.7(c)); whereas increasing input frequency from 300 to 500 Hz increased both power consumptions, probably resulting from the decrease in reactant conversions (Figure 4.7(a)). In addition, a dramatic coke formation might lead to the increase in both power consumptions in this input frequency range. Hence, the minimum power consumptions were found at the input frequency of 300 Hz, and it was selected for further investigation.

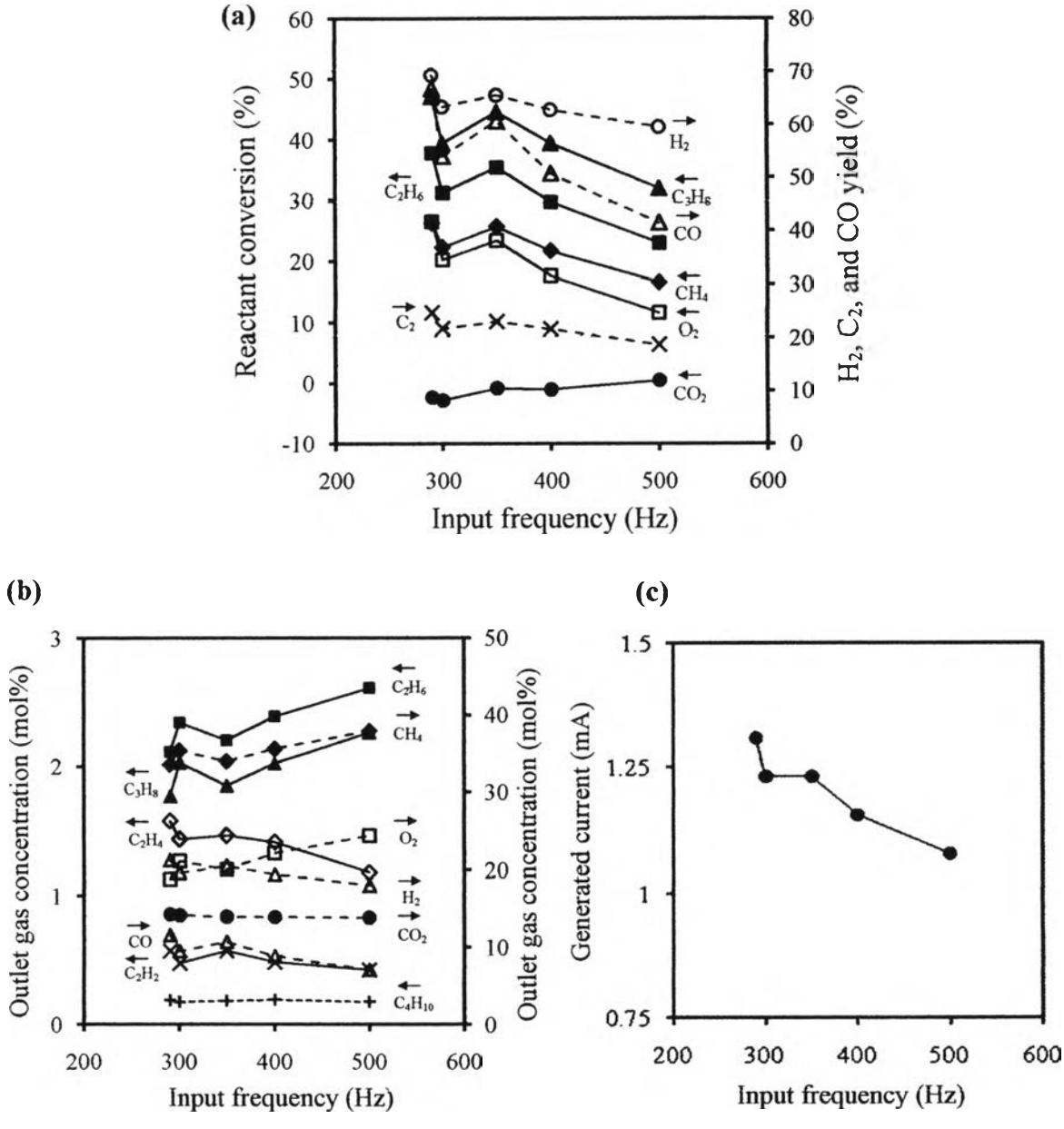


**Figure 4.7** Effect of input frequency on (a) reactant conversions and product yields, (b) concentrations of outlet gas, and (c) generated current for the combined steam reforming and partial oxidation of natural gas (steam content, 10 mol%; $HCs/O_2$ feed molar ratio of 2/1; total feed flow rate, 100 $cm^3$/min; applied voltage, 14.5 kV; and electrode gap distance, 6 mm).

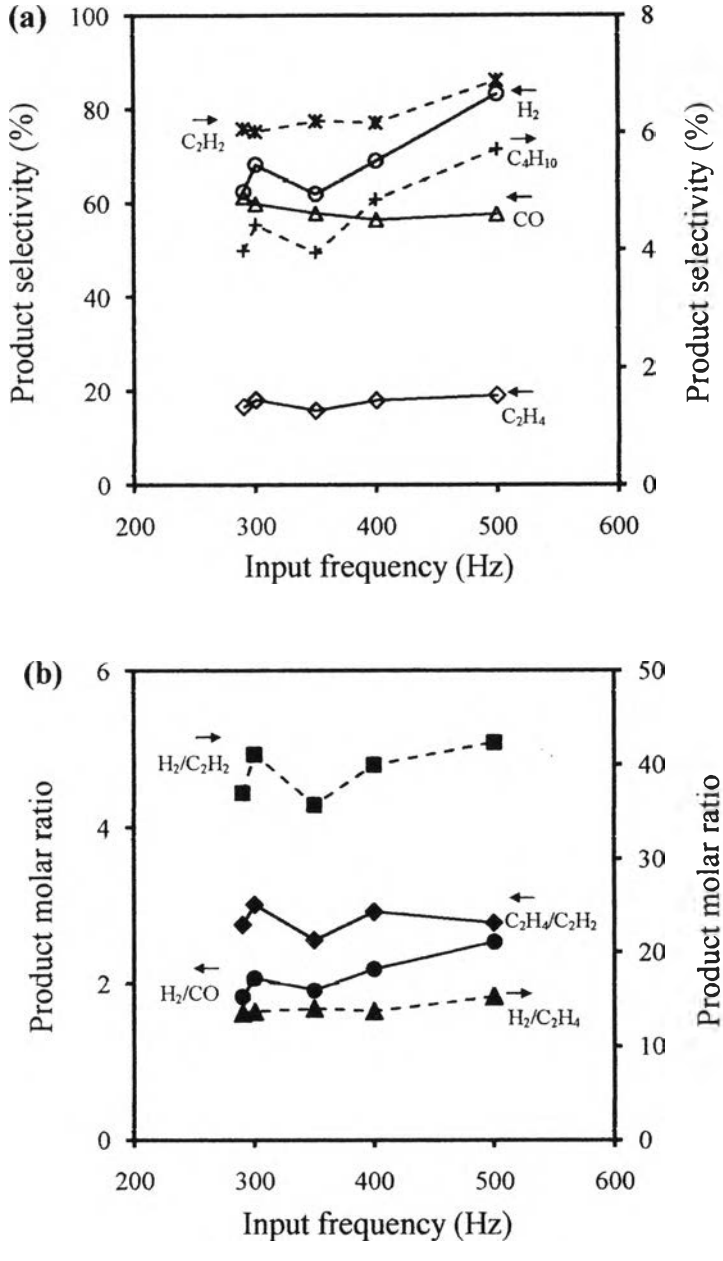


**Figure 4.8** Effect of input frequency on (a) product selectivities and (b) product molar ratios for the combined steam reforming and partial oxidation of natural gas (steam content, 10 mol%; HCs/$O_2$ feed molar ratio of 2/1; total feed flow rate, 100 $cm^3$/min; applied voltage, 14.5 kV; and electrode gap distance, 6 mm).

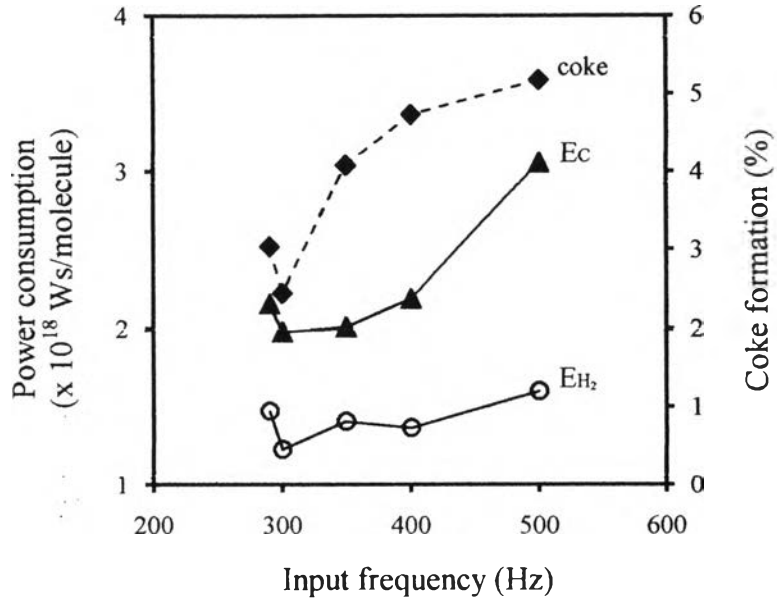


**Figure 4.9** Effect of input frequency on power consumptions and coke formation for the combined steam reforming and partial oxidation of natural gas (steam content, 10 mol%; $HCs/O_2$ feed molar ratio of 2/1; total feed flow rate, 100 $cm^3$/min; applied voltage, 14.5 kV; and electrode gap distance, 6 mm) ($E_C$: power per reactant molecule converted; $E_{H2}$: power per $H_2$ molecule produced).

## 4.4 Effect of Electrode Gap Distance

### 4.4.1 Effect on Reactant Conversions and Product Yields

For the investigation of the effect of electrode gap distance on the reforming reactions of the simulated natural gas, the electrode gap distance was varied in the range of 4-8 mm, while the other operating parameters were controlled at a steam content of 10 mol%, a $HCs/O_2$ feed molar ratio of 2/1, a total feed flow rate of 100 $cm^3$/min, an applied voltage of 14.5 kV, and an input frequency of 300 Hz. In this plasma system, the highest electrode gap distance of 8 mm was limited by the unstable gliding arc discharges, whereas the lowest electrode gap distance of 4 mm was limited by the sudden formation of coke filament across the two electrodes in a relatively short operation period.

The effect of electrode gap distance on the reactant conversions and product yields is shown in Figure 4.10(a). The conversions of $CH_4$, $C_2H_6$, $C_3H_8$, and $O_2$, as well as the $H_2$, CO and $C_2$ yields, significantly increased with increasing electrode gap distance from 4 to 7 mm and then only slightly increased with further increasing electrode gap distance to 8 mm. The increase in the electrode gap distance simply increases the reaction volume and therefore the residence time of gaseous species in the plasma zone. As a result, there are more efficient collisions between reactant molecules and electrons, causing higher conversions of all reactants. These results agree well with the decreases in $CH_4$, $C_2H_6$, $C_3H_8$, and $O_2$ concentrations in the outlet gas (Figure 4.10(b)). Even though the generated current was lower at a higher electrode gap distance (Figure 4.10(c)), the observed higher reactant conversions indicate the more significant role of residence time in enhancing the plasma reactions.

### 4.4.2 Effect on Product Selectivities and Product Molar Ratios

Figure 4.11(a) shows the effect of electrode gap distance on the product selectivities. The $H_2$ selectivity significantly decreased with increasing electrode gap distance. This result indicates that the oxidative dehydrogenation reactions prefer to occur at small electrode gap distance. In addition, the $C_2H_2$ selectivity initially decreased with increasing electrode gap distance from 4 to 6 mm

even though the $C_2H_4$ and $C_4H_{10}$ selectivities increased. It can be implied that the coupling reactions to obtain $C_2H_4$ and $C_4H_{10}$ more preferably occur than the oxidative dehydrogenation reactions. Furthermore, when increasing electrode gap distance from 6 to 8 mm, the $C_2H_2$, $C_2H_4$, and $C_4H_{10}$ selectivities became almost unchanged probably due to the decrease in generated current (Figure 4.10(c)) and the drastic increase in coke formation, as shown next. Besides, the CO selectivity slightly varried with increasing electrode gap distance. Figure 4.11(b) shows the effect of electrode gap distance on the product molar ratios. The molar ratios of $H_2/CO$, $H_2/C_2H_2$, and $H_2/C_2H_4$ greatly decreased with increasing electrode gap distance from 4 to 6 mm and then only slightly decreased with further increasing electrode gap distance to 8 mm, whereas the $C_2H_4/C_2H_2$ molar ratio showed the opposite trend. These results agree well with the trends of product selectivities.

### 4.4.3 Effect on Power Consumptions

Figure 4.12 shows the effect of electrode gap distance on power consumptions and coke formation. The power consumptions both per reactant molecule converted and per $H_2$ molecule produced initially decreased with increasing electrode gap distance from 4 to 6 mm and then tended to slightly increase with further increasing electrode gap distance to 8 mm. The initial decrease in both power consumptions can be explained by the increases in the $CH_4$, $C_2H_6$, $C_3H_8$, and $O_2$ conversions, as well as the $H_2$ yield (Figure 4.10(a)). Even though the minimum power consumptions were found at the electrode gap distance of 6 mm, the reactant conversions and desired product yields at this electrode gap distance were comparatively lower than those at the electrode gap distances of 7 and 8 mm. However, the extremely large coke formation was observed at the electrode gap distance of 8 mm, it was therefore not suitable for operating the plasma reactor. Instead, the electrode gap distance of 7 mm was considered to be the optimum value because it gave the acceptably high reactant conversions and desired product yields, as well as comparatively low power consumptions.

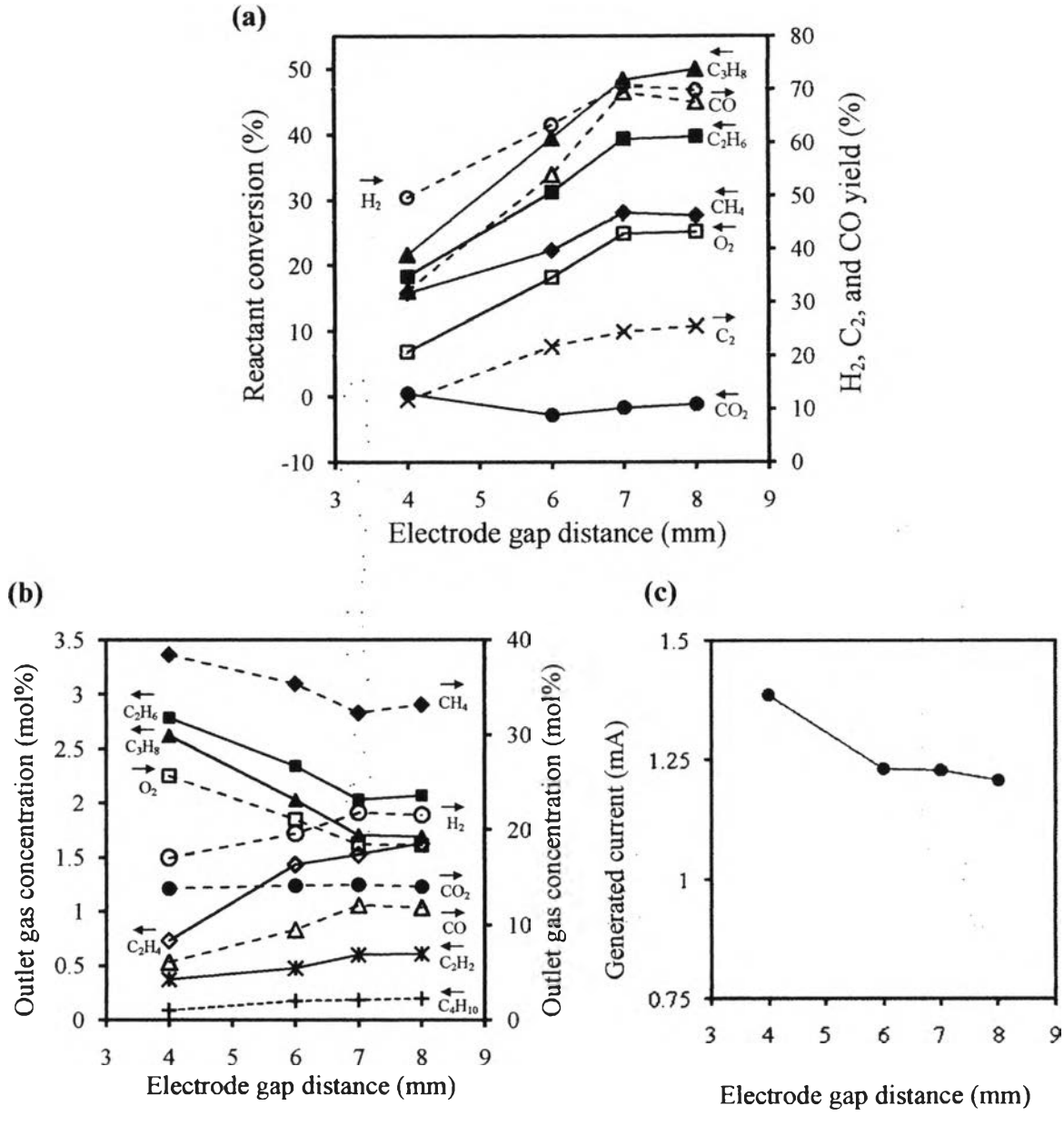


**Figure 4.10** Effect of electrode gap distance on (a) reactant conversions and product yields, (b) concentrations of outlet gas, and (c) generated current for the combined steam reforming and partial oxidation of natural gas (steam content, 10 mol%; HCs/$O_2$ feed molar ratio of 2/1; total feed flow rate, 100 $cm^3$/min; applied voltage, 14.5 kV; and input frequency, 300 Hz).

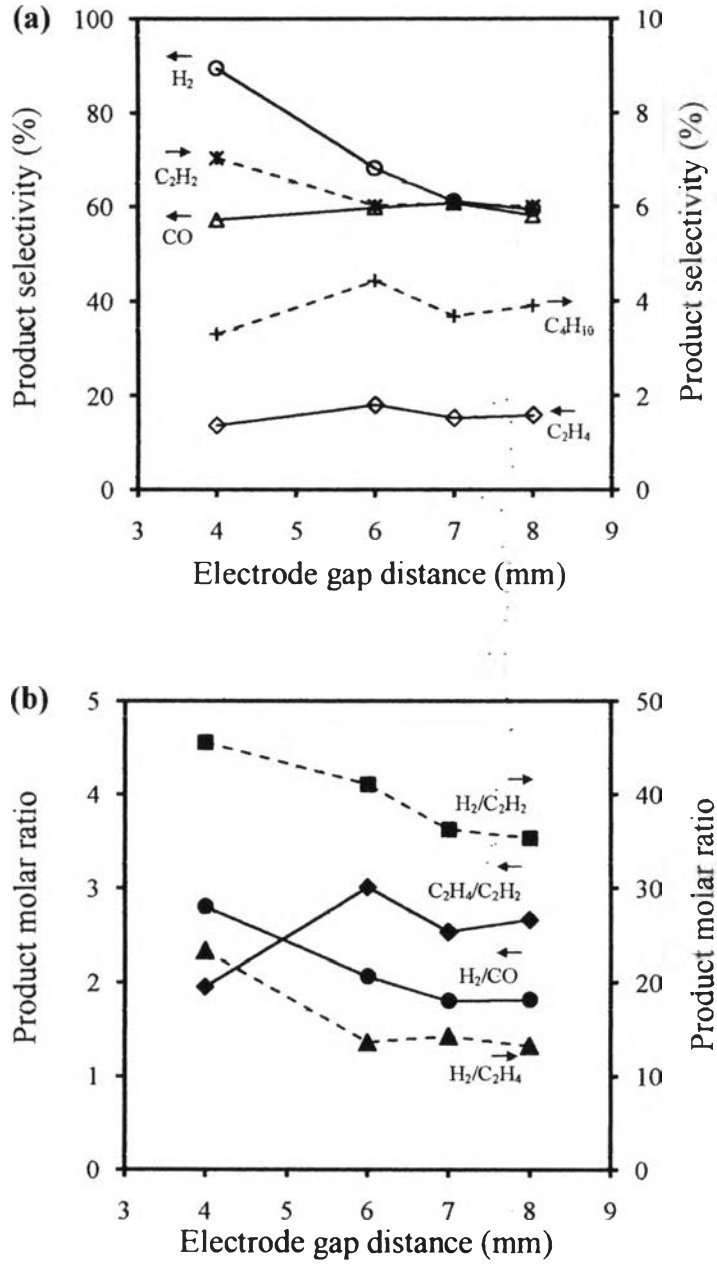


**Figure 4.11** Effect of electrode gap distance on (a) product selectivities and (b) product molar ratios for the combined steam reforming and partial oxidation of natural gas (steam content, 10 mol%; $HCs/O_2$ feed molar ratio of 2/1; total feed flow rate, 100 $cm^3$/min; applied voltage, 14.5 kV; and input frequency, 300 Hz).

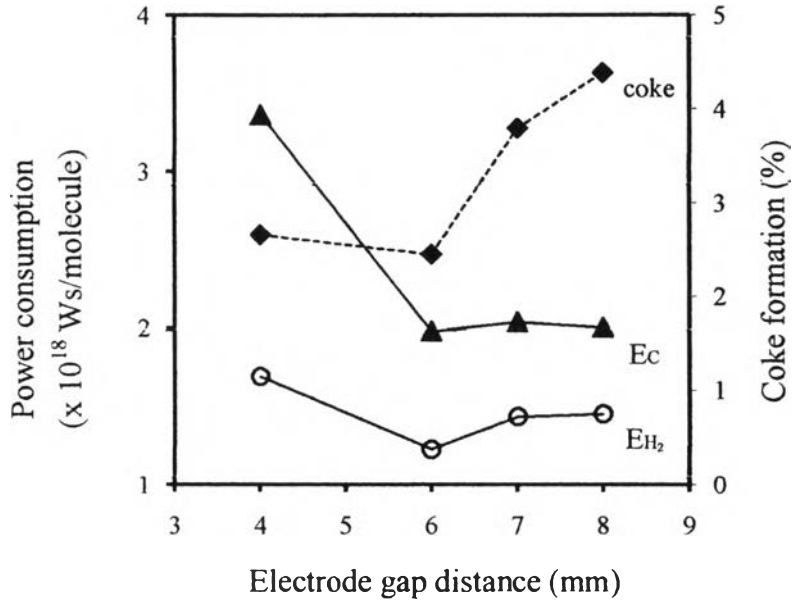


**Figure 4.12** Effect of electrode gap distance on power consumptions and coke formation for the combined steam reforming and partial oxidation of natural gas (steam content, 10 mol%; $HCs/O_2$ feed molar ratio of 2/1; total feed flow rate, 100 $cm^3/min$; applied voltage, 14.5 kV; and input frequency, 300 Hz) ($E_C$: power per reactant molecule converted; $E_{H2}$: power per $H_2$ molecule produced).